Accepted Manuscript

Design, synthesis and biological evaluation of 5-benzylidene-2-iminothiazolidin-4-ones as selective GSK-3β inhibitors

Minhajul Arfeen, Shweta Bhagat, Rahul Patel, Shivcharan Prasad, Ipsita Roy, Asit K. Chakraborti, Prasad V. Bharatam

PII: S0223-5234(16)30392-0

DOI: 10.1016/j.ejmech.2016.04.075

Reference: EJMECH 8604

To appear in: *European Journal of Medicinal Chemistry*

Received Date: 7 March 2016

Revised Date: 26 April 2016

Accepted Date: 28 April 2016

Please cite this article as: M. Arfeen, S. Bhagat, R. Patel, S. Prasad, I. Roy, A.K. Chakraborti, P.V. Bharatam, Design, synthesis and biological evaluation of 5-benzylidene-2-iminothiazolidin-4-ones as selective GSK-3β inhibitors, *European Journal of Medicinal Chemistry* (2016), doi: 10.1016/j.ejmech.2016.04.075.

Graphical Abstract

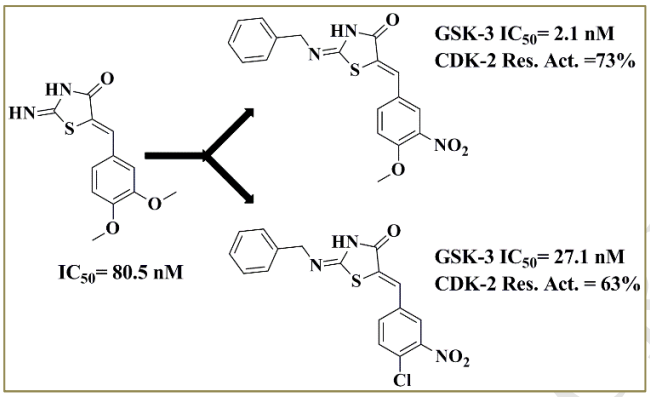

ELSEVIER

European Journal of Medicinal Chemistry
journal homepage: www.elsevier.com

Design, synthesis and biological evaluation of 5-benzylidene-2-iminothiazolidin-4-ones as selective GSK-3β Inhibitors

Minhajul Arfeen,[a] Shweta Bhagat,[a] Rahul Patel,[a] Shivcharan Prasad,[b] Ipsita Roy,[b] Asit K. Chakraborti[a] and Prasad V. Bharatam*[a]

[a]*Department of Medicinal Chemistry, National Institute of Pharmaceutical Education and Research, Sector 67, S.A.S. Nagar160062, Punjab, India*
[b]*Department of Biotechnology, National Institute of Pharmaceutical Education and Research, Sector 67, S.A.S. Nagar160062, Punjab, India*

ARTICLE INFO

Article history:
Received
Revised
Accepted
Available online

Keywords:
GSK-3
CDK-2
Molecular Docking
Molecular Dynamics
SBDD

ABSTRACT

In this work, iminothiazolidin-4-one derivatives were explored as selective GSK-3β inhibitors. Molecular docking analysis was carried to design a series of compounds, which were synthesized using substituted thiourea, 2-bromoacetophenones and benzaldehydes. Out of the twenty five compounds synthesized during this work, the *in vitro* evaluation against GSK-3 led to the identification of nine compounds with activity in lower nano-molar range (2-85 nM). Further, *in vitro* evaluation against CDK-2 showed five compounds to be selective towards GSK-3.

Alzheimer's disease is a neurodegenerative disorder affecting 46.8 million people across the globe.[1] The disease is characterized by progressive cognitive decline such as loss of memory and orientation capability. Glycogen Synthase kinase-3β (GSK-3β), also called as tau phosphorylating kinase, has been targeted for development of therapeutic agents which can be used for treatment of the Alzheimer's disease.[2] GSK-3β, is a protein kinase was originally identified and named for its ability to inactivate the enzyme glycogen synthase.[3] It is a proline directed serine threonine kinase found abundantly in the neurons of the brain.[4] Besides treatment of Alzheimer's disease, GSK-3 has also been targeted for the development of novel therapeutic agents for Type-II diabetes, CNS disorders, chronic inflammatory disorders, malaria and cancer.[5]

Figure 1. Five membered rings reported as GSK-3β inhibitors (**1-13**).

Among the various strategies that have been used for the inhibition of GSK-3β, ATP competitive inhibition has been extensively explored. Several known GSK-3β inhibitors carry 5-membered heterocyclic rings (Figure 1) with hydrogen bond acceptor and donor functionalities. These include 1,2,4-dithiazolidin-3,5-dione (**1**), 1,2,4,-triazoldin-3,5-dione (**2**), 1H-pyrrol-2,5-dione (**3**), 5-imino-1,2,4-thiadiazolidin-3-one (**4**), 1,2,4-thiadiazol-3,5-diamine (**5**), 5-amino-1,2,4-thiadiazol-3(2H)-one (**6**), 1,2,4-thiadiaz-5(2H)-imine (**7**) imidazolidin-2,4-dione (**8**), 2-thioxothiazolidin-4-one (**9**), pyrrolidin-2-one (**10**), 2-thioxoimidazolidin-4-one (**11**), thiazolidin-2,4-dione (**12**), and 1,3,4-oxadiazole (**13**). Compounds containing ring systems (**1-7**) have been reported as substrate competitive or ATP non-competitive inhibitors of GSK-3β by Martinez et al.[6] Hydantoins (**8**) were first reported as GSK-3β ATP competitive inhibitors by Khanfar et al. through in silico screening. Further they identified several potent compounds with five membered heterocyclic scaffolds such as hydantoins (**8**), rhodanines (**9**) and pyrrolidin-2-ones (**10**) through pharmacophore modeling and virtual screening.[7] Saitoh et al. reported oxadiazoles as potent GSK-3β inhibitors.[8] Taking clues from the above mentioned reports, it was found worth exploring the chemical space associated with five membered heterocyclic rings as head groups to design new GSK-3 inhibitors[9].

Figure 2 Flow diagram representing the approach utilized for the design of 2-iminothiazolidin-4-one as GSK-3β ATP competitive inhibitors.

Figure 3. Different subpockets in the ATP binding region of GSK-3β along with AMP-PNP (Pdb code 1PYX).

Computer assisted structure based drug design (SBDD) is a proven strategy for the rational development of small molecules of therapeutic interest without necessitating its synthesis at the preliminary stages. In this method, the available data from X-ray co-crystallized structures is utilized to enhance the pace of drug discovery. Till date, forty seven crystal structures have been reported for GSK-3β. Among these, more than forty co-crystallized structures are reported with ATP

competitive inhibitors. Similarly, more than 150 co-crystallized structures are reported for CDK-2. Despite this wealth of structural information, the role of SBDD has been limited to suggest the analogues of existing leads and to post-rationalize the bioactivity data. Therefore, in this work, molecular docking guided SBDD, synthesis, biological evaluation and molecular dynamics simulations were carried out to identify 2-iminothiazolidin-4-one as selective GSK-3β ATP competitive inhibitors carrying heterocyclic five membered rings.

Rational Design: Figure 2 represents the strategy utilized to identify the 2-iminothiazolidin-4-ones as selective GSK-3β inhibitors. ATP binding pocket of the kinases can be generally divided into four subpockets, namely: (i) solvent accessible region, (ii) hinge region, (iii) hydrophobic back pocket, which is guarded by a gate keeper residue and (iv) polar region (phosphate binding region) as shown in Figure 3 along with AMP-PNP.[10] The most important subpocket of ATP binding domain is hinge region, which is responsible for molecular recognition. Any side chain extending towards the polar region contributes to an increase in potency, whereas side chains extending to the solvent accessible region or towards the hydrophobic back pocket contributes to the selective inhibition of GSK-3β. Two factors were generally held responsible for selective inhibition of GSK-3β in the literature (i) the interactions with amino acids that are unique to GSK-3β active site[11] and (ii) the larger size of the ATP binding cavity in GSK-3β when compared to its homologous counterparts (≈25 kinases).[12] The residues reported for selective inhibition of GSK-3β are Leu132 (Phe80 in CDK-2), Tyr134 (Phe82 in CDK-2), Arg141 (Lys89 in CDK-2) and Cys199 (Ala144 in CDK-2). The larger size of the ATP binding domain in GSK-3β has been attributed to the presence of Leu132. The corresponding residue in case of CDK-2 is Phe80, which does not allow the binding of bulkier group in its surroundings. Another factor contributing to the larger size is the orientation of Arg141 side chain, which points away from the cavity. In case of CDKs, Lys89 at a similar position points inwards and interacts with Ile10 of the glycine rich loop. Similarly the orientation of Asp200 side chain is away from the ATP binding cavity of GSK-3β, whereas in case of CDKs the side chain of Asp at a similar position is directed towards the cavity. As per the literature reports, the selectivity of the 6-bromoindirubins and thiazole-methoxybenzyl-thiourea is due to the presence of Leu132 and orientation of Arg141 respectively.[13] Therefore, the design strategy for the identification of novel GSK-3β inhibitors was divided into three steps (i) identification of hinge binding fragments, (ii) identification of fragments which can access the polar region and (iii) identification of fragments that can bind to solvent accessible region.

Figure 4. Fragments considered for the binding to hinge region. Fragments were screened on the basis of interaction with Asp133 and Val135.

Identification of Hinge Binding Fragments: The crystal structure analysis showed that in majority of co-crystallized complexes the ATP competitive inhibitors formed hydrogen bond interactions with two residues Asp133 and Val135 in the hinge region.[13b, 14] Moreover, literature search on the ATP competitive inhibitors of GSK-3β, CDK-2 and CDK-5 (phylogenetically most closely related kinase to GSK-3β) showed requirement of hydrogen bond acceptor and hydrogen bond donor in *cis* orientation. In light of the above observations, potential hinge binding fragments (**HF-1** to **HF-7**) with hydrogen bond acceptor and donor groups in *cis* orientation were identified during the design, novel GSK-3β inhibitors (Figure 4) were docked into the hinge region of the ATP binding domain of GSK-3β using the protein structure with PDB code 1Q5K. Figure S1 (see Supporting Information) shows the docking results of the hinge binding fragments (**HF-1** to **HF-7**). Top three binding poses of all the fragments were considered for the analysis of docking results. Only those fragments were considered for further evaluation which showed a minimum of two hydrogen bond interactions with hinge binding residues (either Val135 or both Asp133 and Val135). Therefore, -NH hydrogen of **HF-1**, **HF-2**, **HF-3**, and **HF-5** showed hydrogen bond interaction with carbonyl oxygen of Val135, whereas the carbonyl oxygen of these hinge binding fragments showed hydrogen bond contact with NH of Val135. For fragments **HF-4**, and **HF-7** the two hydrogen bond contacts were observed with the Asp133 and Val135 i.e. hydrogen of 'NH' (NH_2 in case of **HF-4**) making hydrogen bond contact with carbonyl oxygen of Asp133 and carbonyl oxygen of fragment making hydrogen bond contact with the NH of Val135. The fragment **HF-6** showed only one desired hydrogen bond contact i.e. hydrogen of the ring 'NH' making hydrogen bond contact with carbonyl oxygen of Val135 and hence, it was not considered for any further study. In addition, careful examination of docking results of these fragments suggested that **HF-5** binds with a pose, in which the methylene carbon and the imine nitrogen can be substituted to access the polar region and solvent accessible regions of the ATP binding domain respectively. Therefore, **HF-5** was selected for the design of novel lead compounds.

Figure 5. Fragments considered for the docking study into the polar binding region of ATP competitive inhibitors.

Identification of Fragments Binding to Polar Region: For the identification of fragments that can bind to polar region, phenyl ring substituted with polar functionalities was chosen. Figure 5 and Figure S2 (supporting information) show the fragments considered and docking results of the fragments binding to the polar region respectively. As mentioned in the previous section, top three binding poses were considered for the docking result analysis. Only those fragments were considered for evaluation which showed hydrogen bond interaction with either the side chain of Lys85 and backbone NH of Asp200 from the DFG loop or with Lys85 or -NH of Asp200 from DFG loop. Therefore, **FG-2**, **FG-5**, **FG-8**, **FG-10**, **FG-13**, **FG-15** and **FG-23** showed hydrogen bond interaction with Lys85 whereas **FG-6**, **FG-9**, **FG-14**, **FG-17**, **FG-18**, **FG-19** and **FG-20** were found to be involved in hydrogen bond interaction with the side chain of Lys85 and NH of Asp200. Furthermore, **FG-1** and **FG-25** showed hydrogen bond contact with Asp200, while **FG-3**, **FG-4**, **FG-11**, **FG-12**, **FG-16** and **FG-21** did not show desired binding pose. Finally, eighteen fragments (**FG-1**, **FG-2**, **FG-5**, **FG-6**, **FG-8**, **FG-9**, **FG-10**, **FG-13**, **FG-14**, **FG-15**, **FG-17**, **FG-18**, **FG-19**, **FG-20**, **FG-22**, **FG-23**, **FG-24** and **FG-25**) were considered for further design of GSK-3β ATP competitive inhibitors.

Figure 6. Structures of the designed first and second series of compounds.

Design of Novel GSK-3β Inhibitors: The molecular docking studies in hinge binding fragments and polar region led to the identification of the heterocycle **HF-5** and eighteen polar fragments. The identified fragments were joined with the exocyclic double bond (Figure S3, supporting information) so as to maintain the co-planarity of the rings, thus designing the first series of compounds (**14**, Figure 6). The designed compounds were evaluated for their binding pose using Glide and FlexX (implemented in SYBYL 7.1) molecular docking programs using crystal structure with PDB code 1Q5K. The cross docking experiments using crystal structure with PDB code 4ACC were also performed to reconfirm the reliability of binding pose. The compounds were evaluated on the basis of hydrogen bond interaction with hinge residues and polar region (as mentioned above). The docking results of the designed compounds showed that the binding pose of the fragment **HF-5** was retained in all the cases, while in case of fragments binding to the polar region though the binding pose was retained, variation in terms of hydrogen bonds was observed.

The designed compounds carry 5-arylidene-2-iminothiazolidin-4-one functional unit in the core of the molecules. A substructure of these molecules i.e. 2-iminothiazolidin-4-one is expected to interact with the hinge binding residues which are important for molecular recognition. This functional unit is already reported to be of considerable therapeutic importance and is known to exhibit anti-inflammatory (**I**),[15] anti-microbial (**II**),[16] and anti-tumor properties (**III**)[17] (Figure S7, supporting information). Several tautomers of this functional unit are also known and reported for various drug discovery efforts (**IV**-**VII**, Figure S7, Supporting information).[18] It is interesting to note that compounds with both these tautomeric scaffolds are of therapeutic importance. In the designed compounds also the tautomerism is possible. To evaluate this, quantum chemical calculations at B3LYP/6-31+G(d) level were carried out which indicated imine tautomer is marginally (1.77 kcal/mol) less stable in **14** (vide infra). The molecular docking results of the two tautomers indicated imine form to be more favourable for interactions with Val135. Hence, substitution at sp^2 nitrogen atom was considered for further evaluation. The quantum chemical calculations showed that in case of phenyl and benzyl substituted derivatives imine tautomer was favoured by 4.91 and 1.87 kcal/mol respectively (Figure S8, supporting information). The crystal structure analysis further showed that only three classes of molecules i.e. analinomaleimide (PDB code 1Q4L),[19] ARA014418 (PDB code 1Q5K)[13b] and pyrazines (4ACD, 4ACC, 4ACG, 4ACH)[20] efficiently exploited the solvent accessible region using phenyl group. Therefore, phenyl and related benzyl group were selected for the design of new series of compounds (**15**, Figure 6) which can bind to three regions (hinge region, polar region and solvent accessible region) of ATP binding domain.

Scheme 1. Reagents, conditions and yields (i) CH_3COOH, CH_3COONa, reflux, 72 h, Yield 40-75%.

Synthesis and Biological Evaluation: Based on the docking scores and binding mode analysis, twelve molecules (**14a**-**l**) were selected for synthesis in the first series (Scheme 1). The synthetic scheme utilizes sodium acetate catalyzed condensation of substituted benzaldehydes (**16**) with 2-imino-4-thiazolidinone (**17**) in acetic acid under reflux condition.[21] Geometrical isomerism (*E*/*Z*) is possible because of the restricted rotation around exocyclic C=C double bond. However, regioselective formation of the *Z* isomer, was confirmed through chemical shift values in 1H NMR (δ_H 7.53-7.58 ppm). The expected chemical shift of the *E* isomers is 6.20–6.30 ppm.[22] The downfield shift of 'H' in the *Z*-isomer is attributed to the anisotropic effect of the nearby C-4 carbonyl group. The synthesized compounds were tested for their inhibitory activity against GSK-3β using a commercially available assay system, based on Z′-LYTE technology, available from invitrogen Life Technologies using human recombinant GSK-3β as the enzyme source.[7b, 23] Two (**14a**, **14c** and **14l**) out of twelve synthesized compounds showed more than 50% inhibitory activity at 0.5 μM, and were evaluated for their IC_{50} values. In this process, two compounds (**14a** and **14l**), with IC_{50} values 80.5 and 84.8 nM respectively, were identified as GSK-3β inhibitors.

Scheme 2. Reagents, conditions and yields (i) DCM, NH_4OH, rt, 2 h, 81% and 83% (ii) EtOH, CH_3COONa, reflux, 6 h, 73% and 77% (iii) CH_3COOH, CH_3COONa, reflux, 72 h, 30-40%.

Thirteen compounds were selected for synthesis from second series (Scheme 2) after performing molecular docking analysis. The hydrogen atom of the imino group in the new set of compounds was substituted with phenyl or benzyl groups to gain access to the solvent accessible region of the ATP binding cavity. The compounds substituted with hydroxy, methoxy, halogen and nitro at 3rd and 4th positions of the benzylidine ring were considered for synthesis. The starting material for the synthesis of the desired compounds was obtained by the treatment of phenyl and benzyl isothiocynates (**18**) with 24% solution of aqueous ammonia. The precipitated thiourea (**19**) was heated under reflux with α-chloroethylacetate (**20**) in the presence of sodium acetate in ethanol to obtain the substituted 4-iminothiazolidinone derivatives (**21**). The substituted 4-iminothiazolidinone was heated under reflux conditions with substituted benzaldehydes and sodium acetate in acetic acid to obtain the desired products. The synthesized compounds were evaluated for their GSK-3β inhibitory activity as mentioned above (Figure S11, supporting information). Seven out of thirteen synthesized compounds showed more than 50% inhibition at 0.5 μM. The identified compounds were then evaluated for their IC_{50} values (Table 1). The lowest value was found to be 2.1 nM (**15g**) while the highest was found to be 51.7 nM (**15k**).

Table 1. IC_{50} values for GSK-3β and percentage residual activity of CDK-2 for seven compounds at 2 μM Inhibitor concentration. The activity of CDK-2 in the absence of inhibitor was assigned the value of 100%.

Earlier, in 2007 Richardson et al. reported 2-iminothiazolidin-4-ones as potent CDK-2 inhibitors. While screening for selective inhibition of CDK-2, five compounds showed non-selective inhibition and one compound showed selective inhibition for GSK-3β.[24] Similarly, in 2012, Bazureau et al. reported a closely related 2-amino-thiazole-4-one derivative as possible kinase inhibitor.[18a] The newly designed compounds (Table 1) are significantly more active than the reported compounds. Moreover, all the compounds reported from this work fit comfortably into the ATP binding domain. CDK-2 is the most closely related kinase to GSK-3β with an overall similarity of 33% (98% similarity in ATP binding domain). Even the most selective inhibitors of GSK-3β reported so far inhibit CDK-2,

therefore, CDK-2 was chosen to evaluate the selectivity of inhibitors. The identified hits should show the low inhibition of CDK-2 to avoid possible adverse effects. The seven identified compounds (**15a**, **b**, **e**, **f**, **g**, **k**, **l**) were evaluated for selectivity against CDK-2 at 2 μM concentration, five of them showed significant selectivity for inhibition of GSK-3β (> 60% residual activity for CDK-2), the highest being shown by **15g** (Table 1). The experimentally observed selective affinity of these inhibitors for GSK-3β can be attributed to the following two reasons (i) Arg141 forms salt bridge interaction with Glu137 and hence defines the periphery and entry region of the ATP binding pocket. Residues at similar position in case of CDK-2, involved in the salt bridge formation are Lys89 and Glu85. The side chain of the Lys89 points inwards and interacts with the backbone atom of Ile10. This arrangement would not allow the occupancy of the phenyl or benzyl group in case of CDK-2. (ii) Difference in the gate keeper residue which is Leu132 in case of GSK-3 and Phe80 in case of CDK-2. The presence of Phe80 does not allow the accommodation of substituted benzylidene ring around the polar region. However, the docking study suggests that this group fits elegantly into the GSK-3β ATP binding site (Figure 7 and Figure S5, see supporting information).

Figure 7. Docked pose of **15g** and bar diagram represents the per residue wise decomposition analysis, residues on the X-axis, whereas Energy (kcal/mol) is on Y-axis.

Molecular Dynamics Simulations: To gain further insights into the selective inhibition of GSK-3β, molecular dynamics simulations for 24 ns were carried out for **15g** (most active and selective) in complex with GSK-3β and CDK-2. The MM-GBSA energy decomposition analysis and residue wise energy decomposition were performed using a python script of AMBER 11.0 program. The RMSD analysis for the two complexes showed that systems attained equilibrium within 2 ns of simulation run (Figure S9, supporting information). The binding free energy calculations showed a difference of 4.10 kcal/mol (solvent phase) in favor of GSK-3β (Figure S10, Table S1, supporting information) with respect to CDK-2. The energy decomposition analysis showed that the van der Waals energy favored the binding of **15g** to GSK-3β by 3.22 kcal/mol.

The electrostatic energy resists the binding of **15g** to GSK-3β by 2.30 kcal/mol under gas phase while the same favors binding of **15g** to GSK-3β under solvent condition by ~1 kcal/mol. Residue wise energy decomposition analysis was also taken up to identify key residues that play a detrimental role in selective inhibition of GSK-3β over CDK-2 (Figure 7, Table S2, supporting information). The interactions were quantified in terms of pair wise interaction decomposition of free energy. The important residues found to be participating in GSK-3β inhibitor interaction (cut off value 0.5 kcal/mol) are Ile62, Val70, Ala83, Lys85, Leu132, Tyr134, Val135, Glu137, Thr138, Arg141, Asn186, Leu188, Cys199, and Asp200 (for CDK-2, the equivalent amino acids are Ile10, Val18, Ala31, Lys33, Phe80, Phe82, Leu83, Gln85, Asp86, Lys89, Asn132, Leu134, Ala144 and Asp145). The amino acids Ile10 (Ile62), Val70 (Val18), Ala83 (Ala31), Leu132 (Phe80), Tyr134 (Phe82), Val135 (Leu83), Glu137 (Gln85), Thr138 (Asp86), Asn186 (Asn132), Leu188 (Leu134), Asp200 (Asp145) showed similar strength of interaction (0.5 to 2 kcal/mol). The residues Lys85, Thr138, Arg141 and Cys199 showed the interaction energy of 0.97, 1.13, 1.11 and 1.371 kcal/mol respectively. The interaction energies for the residues at the similar position in case of CDK-2 are 0.057, 0.484, 0.194 (repulsive) and 0.73 kcal/mol respectively. The above analysis clearly indicates that the residues like Arg141, Thr138, Cys199 and interaction with Lys85 in GSK-3β play deterministic role in selective inhibition of GSK-3β.

Discussion

SBDD methods were employed to design 2-iminothiazolidin-4-one class of compounds as potent GSK-3 inhibitors. Synthesis and biochemical evaluation using GSK-3 and CDK-2 assay system lead to the identification of five selective GSK-3 inhibitors. MD simulations on the **15g-GSK-3** and **15g-CDK-2** complexes provided clues towards the observed selectivity. This molecular modelling, synthesis and biochemical study provided an opportunity to explore structure activity relation analysis as discussed below. The comparative analysis of binding mode for **14a-14l** and their tautomers showed that imine tautomer (2-iminothiazolidin-4-one) is essential for the fingerprint H-bond (Val135) for GSK-3β in the hinge region, whereas the 2-aminothiazolidin-4-one was found to make hydrogen bond contacts with Arg141 (solvent accessible region, see Supporting Information). *In vitro* screening of the 12 synthesized compounds from the first series (**14a-14l**) resulted in two compounds with 50% GSK-3β inhibitory activity below 500 nM. The reason for the smaller number of successful compounds from this series can be attributed to the preference of amine tautomer which leads to the variability of binding mode in the ATP binding cavity and thus leading to the instability of inhibitor-GSK-3β complex. This assumption gains strength from the fact that in the second series (**15a-15m**), seven out of the thirteen synthesised compounds were found to show 50% GSK-3β inhibitory activity below 500 nM. This increased number of successful molecules in the second series can be credited to the N-substituted phenyl and benzyl ring, which leads to the greater stability in the binding mode because of the preference for the imine tautomer. Moreover, the above stated substitution resulted into the compounds with higher affinity for GSK-3β (ex. **15l** in comparison to **14a**) however, the high potency of **14a**, **14l**, **15a**, **15b**, **15e**, **15f**, **15g**, **15k** and **15l** can be ascribed to the occupancy of the hydrophobic pocket around polar region by the benzylidene ring. It was further observed that groups capable of making hydrogen bonds (**15a**, **15f**, **15g**, **15k** and **15l**) or halogen bonds (**15b** and **15e**) with Lys85 are preferred at the 4th position. Interestingly both nitro (**15e** and **15g)** and methoxy/ethoxy groups (**15k** and **15l**) were favoured at the 3rd position. Compounds with nitro substitution (24.0 and 2.1 nM) showed higher potency in comparison to compounds with methoxy substitution (51.7 and 44.3 nM). Relative investigation of binding mode revealed that nitro group is involved in the polar interaction with Leu132, whereas methoxy and ethoxy groups are involved in the weak steric clash with Leu132. Besides, nitro group is also involved in polar interaction with Val70 and Asp200. This observation is in accordance with the MD simulation study where Leu132, Val70 and Asp200 (Figure 7) showed interaction energies of ~ 0.58, 1.75 and 0.64 kcal/mol respectively. It is pertinent to mention that **15d** did not show significant GSK-3β inhibitory activity even at 500 nM. It was observed that there exists a strong intramolecular hydrogen bond between nitro and hydroxyl groups, which leads to the co-planarity of nitro group with the benzylidene ring and thus loss of polar contacts with Leu132, Val70 and Asp200. Similarly, **15h** did not show significant inhibitory activity at evaluatory concentration, which can be ascribed to the strong steric clash with Gly65, Val70, Lys85 and Asp200.

Conclusions

In conclusion, SBDD using molecular docking methodology was utilized to design 2-iminothiazolidinones as a new class of GSK-3β inhibitors. The synthesis and *in vitro* biological evaluation resulted in the identification of nine compounds, which showed GSK-3β inhibition in lower nano molar range (lowest being 2.1 nM and highest being 84.8 nM). Five compounds emerged as selective GSK-3β inhibitors against CDK-2. MD simulation study of the most potent as well as selective compound showed that the selectivity of this class of compounds is determined by the residues Lys85, Thr138, Arg141 and Cys199 of GSK-3. Further, this work proves that the above mentioned residues can be effectively utilized to design selective GSK-3β inhibitors.

Experimental Section

General Information:

All starting materials were purchased from Sigma-Aldrich/Alfa Aesar and used further without any additional purification. All reactions were carried out in flame-dried glass wares under N_2. All the compounds (intermediates and final compounds) were purified by column chromatography using silica gel (100-200 mesh) as stationary phase and hexane-ethyl acetate as mobile phase. Proton nuclear magnetic resonance spectra (^{1}H NMR) were recorded on Avance III 400 Bruker (400 MHz). Proton chemical shifts are expressed in parts per million (ppm, δ scale) and are referenced to residual proton in the NMR solvent ($CDCl_3$, δ 7.26, CD_3OD, δ 3.31 and CD_3SOCD_3, δ 2.49). The following abbreviations were used to describe peak patterns when appropriate: br = broad, s = singlet, d = doublet, t = triplet, m = multiplet. Coupling constants, *J*, were reported in Hertz unit (Hz). Carbon 13 nuclear magnetic resonance spectroscopy (^{13}C NMR) was recorded on Avance III 400 Bruker (100 MHz) and was fully decoupled by broad band decoupling. Chemical shifts were reported in ppm referenced to the centre line at a 77.0, 49.0 and 39.7 ppm of $CDCl_3$, CD_3OD and CD_3SOCD_3 respectively. High resolution mass spectra were taken with Maxis-Bruker using ESI-TOF method.

Experimental Procedures for Synthesized Compounds

Preparation of compound 14a: To the magnetically stirred solution of **17** (232 mg, 2 mmol) in HOAc (7 mL), was added NaOAc (500 mg, 6 mmol). After 15 min 3,4-dimethoxybenzaldhyde (**16a**, 400 mg, 2.4 mmol) was added and the reaction mixture was heated under reflux for 72 h. The HOAc was removed under reduced pressure and the resultant solid was washed successively with water, methanol and EtOAc to obtain the desired products as solid.

5-(3,4-Dimethoxybenzylidene)-2-iminothiazolidin-4-one (14a): Yellow solid; mp > 200 ºC; 235 mg, 45% yield; IR (neat) ν_{max} = 3344, 2759, 1720, 1690, 1678 cm^{-1}; ^{1}H NMR (400 MHz, CD_3SOCD_3) δ = 9.35 (s, 1H), 9.09 (s, 1H), 7.54 (s, 1H), 7.08-7.16 (m, 3H), 3.80 (s, 6H); ^{13}C NMR (100 MHz, CD_3SOCD_3): δ = 180.52, 175.39, 149.98, 148.81, 129.42, 126.62, 126.51, 122.77, 112.63, 111.98, 55.57, 55.38; HRMS (ESI-TOF): m/z calculated for $C_{12}H_{12}N_2O_3S$ $[M+Na]^+$, 287.0466; found 287.0461.

5-(3,4,5-Dimethoxybenzylidene)-2-iminothiazolidin-4-one (14b): Yellow solid; mp > 200 ºC; 229 mg, 39% yield; IR (neat) ν_{max} = 3148, 2962, 1667, 1581 cm^{-1}; ^{1}H NMR (400 MHz, CD_3SOCD_3) δ 9.31 (br s, 2H), 7.54 (s, 1H), 6.9 (s, 2H), 3.8 (s, 6H), 3.69 (s, 3H); ^{13}C NMR (100 MHz, CD_3SOCD_3): δ 180.79, 175.88, 153.61, 139.11, 130.11, 129.85, 128.86, 107.38, 60.64, 56.37 HRMS (ESI-TOF): m/z calculated for $C_{13}H_{14}N_2O_4S$ $[M+Na]^+$, 317.0572; found 317.0567.

5-(4-Hydroxy-3-methoxybenzylidene)-2-iminothiazolidin-4-one (14c): Yellow solid; mp > 200 ºC; 215 mg, 43% yield; IR (neat) ν_{max} = 3364, 2955, 1735, 1680, 1584 cm^{-1}; ^{1}H NMR (400 MHz, CD_3SOCD_3) δ 9.76 (s, 1H), 9.29 (br s, 1H), 9.05 (s, 1H), 7.50 (s, 1H), 7.13 (s, 1H), 7.06 (d, *J* = 8.28, 1H), 6.9 (d, *J* = 7.92, 1H); ^{13}C NMR (100 MHz, CD_3SOCD_3): δ 175.91, 148.92, 148.35, 130.35, 125.94, 125.81, 123.69, 116.49, 113.88, 56.00; HRMS (ESI-TOF): m/z calculated for $C_{11}H_{10}N_2O_3S$ $[M+H]^+$, 251.0490; found 251.0491.

5-(4-Hydroxy-3-nitrobenzylidene)-2-iminothiazolidin-4-one (14d): Orange solid; mp > 200 ºC; 330 mg, 61% yield; IR (neat) ν_{max} = 3164, 2772, 1679, 1604 cm^{-1}; ^{1}H NMR (400 MHz, CD_3SOCD_3) δ 9.46 (br s, 1H), 9.18 (s, 1H), 8.05 (s, 1H), 7.75 (d, *J* = 8.74, 1H), 7.55 (s, 1H), 7.24 (d, *J* = 8.72, 1H); ^{13}C NMR (100 MHz, CD_3SOCD_3): δ 180.71, 175.57, 153.52, 137.52, 136.46, 129.04, 127.52, 126.27, 125.66, 120.53 HRMS (ESI-TOF): m/z calculated for $C_{10}H_7N_3O_4S$ $[M+Na]^+$, 288.0055; found 288.0046.

5-(4-Bromo-3-nitrobenzylidene)-2-iminothiazolidin-4-one (14e): Yellow solid; mp > 200 ºC; 334 mg, 51% yield; IR (neat) ν_{max} = 3197, 2761, 2302, 1666, 1613, 1610 cm^{-1}; ^{1}H NMR (400 MHz, CD_3SOCD_3) δ 9.62 (s, 1H), 9.32 (s, 1H), 8.04 (d, *J* = 8.28, 1H), 7.74 (s, *J* = 8.28, 1H), 7.6 (s, *J* = 8.28, 1H); ^{13}C NMR (100 MHz, CD_3SOCD_3): δ 180.28, 175.47, 150.34, 136.00, 135.72, 133.96, 133.49, 126.23, 126.06, 114.00; HRMS (ESI-TOF): m/z calculated for $C_{10}H_6BrN_3O_3S$ $[M+Na]^+$, 349.9211; found 349.9203.

5-(4-Methoxy-3-nitrobenzylidene)-2-iminothiazolidin-4-one (14f): Orange solid; mp > 200 ºC; 301 mg, 54% yield; IR (neat) ν_{max} = 3236, 2951, 1682, 1608 cm^{-1}; ^{1}H NMR (400 MHz, CD_3SOCD_3) δ 9.49 (s, 1H), 9.21 (s, 1H), 8.11 (s, 1H), 7.86 (d, *J* = 8.00 1H), 7.58 (s, 1H) 7.51 (d, *J* = 8.84, 1H) 4.31 (s, 3H); ^{13}C NMR (100 MHz, CD_3SOCD_3): δ 180.62, 175.61, 153.00, 139.71, 135.70, 130.05, 127.13, 125.98, 115.70, 57.51: HRMS (ESI-TOF): m/z calculated for $C_{11}H_9N_3O_4S$ $[M+Na]^+$, 302.0211; found 302.0244.

5-(4-Formylbenzylidene)-2-iminothiazolidin-4-one (14g): Yellow solid; mp > 200 ºC; 315 mg, 68% yield; IR (neat) ν_{max} = 3194, 2995, 1677, 1606 cm^{-1}; ^{1}H NMR (400 MHz, CD_3SOCD_3) δ 10.01 (s, 1H), 9.56 (s, 1H), 9.33 (s, 1H), 8.01 (d, *J* = 7.16, 2H), 7.77 (d, *J* = 7.40, 2H), 7.57 (s, 1H); ^{13}C NMR (100 MHz, CD_3SOCD_3): δ 193.00, 180.49, 175.84, 140.23, 136.39, 133.08, 130.57, 130.34, 128.01; HRMS (ESI-TOF): m/z calculated for $C_{11}H_8N_2O_2S$ $[M+Na]^+$, 255.0204; found 255.0249.

5-(4-Chloro-3-nitrobenzylidene)-2-iminothiazolidin-4-one (14h): Orange solid; mp > 200 ºC; 338 mg, 60% yield; IR (neat) ν_{max} = 3214, 3009, 1965, 1693, 1667 cm^{-1}; ^{1}H NMR (400 MHz, CD_3SOCD_3) δ 9.58 (s, 1H), 9.33 (s, 1H) 8.20 (s, 1H), 7.82-7.89 (m, 2H), 7.62 (s, 1H); ^{13}C NMR (100 MHz, CD_3SOCD_3): δ 180.28, 175.47, 148.21, 135.23, 134.26, 133.46 132.95, 126.39, 125.98, 125.79; HRMS (ESI-TOF): m/z calculated for $C_{10}H_6ClN_3O_3S$ $[M+Na]^+$, 305.9716; found 305.9712.

5-(3-Carboxybenzylidene)-2-iminothiazolidin-4-one (14i): Yellow solid; mp > 200 ºC; 218 mg, 44% yield; IR (neat) ν_{max} = 3278, 3110, 2764, 2413, 1874, 1682, 1641, 1602 cm^{-1}; ^1H NMR (400 MHz, CD_3SOCD_3) δ 9.51 (br s, 1H) 9.21 (s, 1H), 8.51 (s, 1H), 7.97 (d, *J* = 7.60, 1H), 7.84 (d, *J* = 7.48, 1H), 7.64 (s, 1H), 7.62-7.60 (m, 1H); ^{13}C NMR (100 MHz, CD_3SOCD_3): δ 180.65, 175.85, 167.26, 134.97, 134.91, 132.12, 130.97, 130.44, 130.07, 129.32, 128.38; HRMS (ESI-TOF): m/z calculated for $C_{11}H_8N_2O_3S$ $[M+H]^+$, 249.0334; found 249.0328.

5-(3-ethoxy-4-hydroxybenzylidene)-2-iminothiazolidin-4-one (14j): Yellow solid; mp > 200 ºC, 216 mg, 41% yield; IR (neat) ν_{max} = 3395, 3120, 2759, 1689, 1585 cm^{-1}; ^1H NMR (400 MHz, CD_3SOCD_3) δ 12.50 (s, 1H) 9.88 (s, 1H), 7.69 (s, 1H), 7.13 (s, 1H), 7.04 (d, *J* = 7.98, 1H), 6.93 (d, *J* = 8.2, 1H), 4.06-4.05 (m, 2H), 2.07 (s, 1H), 1.34 (t, *J* = 6.92, 3H); ^{13}C NMR (100 MHz, CD_3SOCD_3): δ 168.51, 167.92, 150.11, 147.56, 133.12, 124.80, 124.64, 119.56, 116.69, 115.62, 64.34, 15.07; HRMS (ESI-TOF): m/z calculated for $C_{12}H_{12}N_2O_3S$ $[M+H]^+$, 265.0647; found 265.0637.

5-(4-Carboxybenzylidene)-2-iminothiazolidin-4-one (14k): Yellow solid; mp > 200 ºC; 233 mg, 47% yield; IR (neat) ν_{max} = 3072, 2774, 2418, 1862, 1644 1585 cm^{-1}; ^1H NMR (400 MHz, CD_3SOCD_3) δ 9.52 (br s, 1H), 9.25 (s, 1H), 8.04 (d, *J* = 8.40, 2H), 7.68 (d, *J* = 8.36, 2H), 7.63 (s, 1H), ^{13}C NMR (100 MHz, CD_3SOCD_3): δ 180.52, 175.83, 167.17, 138.70, 132.28, 131.43, 130.44, 129.85, 128.15; HRMS (ESI-TOF): m/z calculated for $C_{11}H_8N_2O_3S$ $[M+H]^+$, 249.0334; found 249.0329.

5-(3-Carboxy-4-hydroxybenzylidene)-2-iminothiazolidin-4-one (14l): Yellow solid; mp > 200 ºC; 153 mg, 29% yield; IR (neat) ν_{max} = 3243, 1654, 1580 cm^{-11}H NMR (400 MHz, CD_3SOCD_3) δ 9.39 (br s, 1H), 9.09 (s, 1H), 8.04 (s, 1H), 7.75 (d, *J* = 8.72, 1H), 7.55 (s, 1H), 7.09 (d, *J* = 8.64, 1H); ^{13}C NMR (100 MHz, CD_3SOCD_3): δ 180.92, 175.77, 171.67, 162.23, 137.86, 132.73, 131.09, 128.66, 127.69, 125.67, 124.63, 118.69, 114.29; HRMS (ESI-TOF): m/z calculated for $C_{11}H_8N_2O_4S$ $[M+H]^+$, 265.0283; found 265.0278.

Preparation of compound 19a: To a magnetically stir solution of phenyl-isothiocyanate (**18-Ph**, 239 µL, 2 mmol) in toluene (5 mL) was added aq. NH_3 solution (417 µL, 6 mmol). The reaction mixture was allowed to stir for 3 h. The precipitated white solid was filtered and washed with diethyl ether to directly use in the next step without any further purification.

Preparation of compound 21a: To a magnetically stirred suspension of phenylthiourea (**19a**, 304 mg, 2 mmol) and anhydrous NaOAc (820 mg, 10 mmol) in absolute ethanol (7 mL) was added ethyl chloroacetate (**20**, 0.5 mL, 4 mmol) and the mixture was heated under reflux for 6 h. The reaction mixture was concentrated under reduced pressure. The residue was diluted with water (50 mL) and extracted with EtOAc (3∗15 mL). The combined EtOAc extracts were dried (anhydrous Na_2SO_4), filtered and the filtrate was concentrated under rotary vacuum evaporator to obtain a solid mass which was recrystallized from EtOAc to obtain the desired product as white solid.

2-(Phenylimino)thiazolidin-4-one (21a): White solid; 347 mg, 90% yield; IR (neat) ν_{max} = 3276, 3210, 3141, 3090, 3011, 2862, 1681, 1637, 1606, 1570 cm^{-1}; ^1H NMR (400 MHz, CD_3SOCD_3) *δ* = 7.69 (d, *J* = 7.52, 1H), 7.38(d, *J* = 7.24, 2H), 7.16 (t, *J* = 7.32, 1H), 7.00(d, *J* = 7.21H), 4.05-3.96 (m, 2H); ^{13}C NMR (100 MHz, CD_3SOCD_3): δ 188.71, 178.71, 139.22, 129.77, 129.50, 125.16, 122.00, 120.71.

2-(Benzylimino)thiazolidin-4-one (21b):white solid; 359 mg, 87% yield, ^1H NMR (400 MHz, CD_3SOCD_3) *δ* = 7.37-7.25 (m, 5H), 4.61 (s, 2H), 3.90 (s, 2H); ^{13}C NMR (100 MHz, CD_3SOCD_3): δ = 187.62, 182.69, 138.03, 137.57, 129.00, 128.94, 128.72, 128.18, 127.99, 127.95, 127.82, 127.79, 48.31.

Preparation of Compound 15a: To the stirred solution of phenyliminothiazolidin-4-one (**21a**, 385 mg, 2 mmol) and 4-hydroxybenzaldehyde (**16a**, 183 mg, 1.5 mmol) in HOAc (5 mL), NaOAc (820 mg, 10 mmol) was added. The reaction mixture was then heated under reflux for 72 h. The reaction mixture was then allowed to cool to room temperature, resulting into the precipitation of yellow solid which was filtered and washed with water, methanol and EtOAc to purify.

5-(4-Hydroxybenzylidene)-2-(phenylimino)thiazolidin-4-one (15a): Pale yellow solid; mp > 200 ºC; 355 mg, 60% yield; IR (neat) ν_{max} = 2951, 2766, 2539, 1725, 1611, 1574, 1526 cm^{-1}; ^1H NMR (400 MHz, CD_3SOCD_3) *δ* = 7.77 (s, 1H), 7.64-7.34 (m, 5H), 7.19 (t, *J* = 7.16, 1H), 7.05 (s, 1H), 6.9 (s, 1H), 6.86 (s, 1H); ^{13}C NMR (100 MHz, CD_3SOCD_3) *δ* = 162.05, 158.12, 151.27, 137.34, 132.06, 130.28, 129.32, 128.65, 123.47, 122.66, 120.89, 115.77, 115.27; HRMS (ESI-TOF): m/z calculated for $C_{16}H_{12}N_2OS$ $[M+Na]^+$, 319.0517; found 319.0511.

5-(4-Fluorobenzylidene)-2-(phenylimino)thiazolidin-4-one (15b): Pale yellow solid; mp > 200 ºC 476 mg, 80% yield; IR (neat) ν_{max} = 3204, 2922, 2854, 1667, 1636, 1598, 1571 cm^{-1}; ^1H NMR (400 MHz, CD_3SOCD_3) *δ* = 7.78 (s, 1H), 7.74 (s, 1H), 7.69-7.67, (m, 1H), 7.64 (s, 1H), 7.58-55 (m, 1H), 7.38-7.46 (m, 2H), 7.31 (t, *J* = 8.6, 1H), 7.21 (t, *J* = 7.2, 1H), 7.06 (d, *J* = 7.48, 1H); ^{13}C NMR (100 MHz, CD_3SOCD_3) *δ* = 164.18, 161.74, 132.53, 131.05, 129.98, 128.77, , 127.63, 125.67, 121.89, 121.10, 116.93, 16.71; HRMS (ESI-TOF): m/z calculated for $C_{16}H_{11}FN_2OS$ $[M+Na]^+$, 321.0474; found 321.0439.

5-(4-Chlorobenzylidene)-2-(phenylimino)thiazolidin-4-one (15c): Yellow solid; mp > 200 ºC; 544 mg, 86% yield; IR (neat) ν_{max} = 3261, 3201, 3140, 2921, 2852, 1665, 1635, 1601, 1588, 1570, 1535 cm^{-1}; ^1H NMR (400 MHz, CD_3SOCD_3) *δ* = 7.76 (s, 1H), 7.18 (s, 1H), 7.64-7.62 (m, 2H), 7.53 (s, 2H), 7.40-7.43 (m, 2H), 7.23-7.20 (m, 1H), 7.06-7.04 (m, 2H); ^{13}C NMR (100 MHz, CD_3SOCD_3) *δ* = 173.97, 134.06, 133.02, 132.50, 131.16, 129.42, 129.28, 129.21, 129.07, 128.36, 127.32, 124.97, 124.82, 124.70, 121.46 120.83; HRMS (ESI-TOF): m/z calculated for $C_{16}H_{11}ClN_2OS$ $[M+Na]^+$, 337.0178; found 337.0142.

5-(4-Hydroxy-3-nitrobenzylidene)-2-(benzylimino)thiazolidin-4-one (15d): yellow solid; mp > 200 ºC; 217 mg, 30% yield; IR (neat) ν_{max} = 3269, 3057, 2757, 1691, 1622, 1602, 1535 cm^{-1}; ^1H NMR (400MHz, CD_3SOCD_3) δ 10.10 (s, 1H), 8.11 (s, 1H) 7.77 (d, *J* = 8.78, 1H), 7.60 (s, 1H), 7.39-7.31 (m, 5H), 7.27 (d, *J* = 8.64, 1H), 4.75 (s, 2H); ^{13}C NMR (100 MHz, CD_3SOCD_3) *δ* = 179.96, 173.81, 153.36, 137.58, 136.36, 129.10, 128.47, 128.18, 128.07, 127.78, 126.42, 125.79, 120.49, 48.28; HRMS (ESI-TOF): m/z calculated for $C_{17}H_{13}N_3O_4S$ [M+Na], 378.0524; found 378.0516.

5-(4-Chloro-3-nitrobenzylidene)-2-(benzylimino)thiazolidin-4-one (15e): Yellow solid; mp > 200 ºC; 195 mg, 26% yield; IR (neat) ν_{max} = 3211, 3060, 2770, 1693, 1635, 1610, 1532 cm^{-1}; ^1H NMR (400MHz, CD_3SOCD_3) δ 8.27 (s, 1H), 7.85-7.92 (m, 2H), 7.68 (s, 1H), 7.37-7.40 (m, 5H), 4.77 (s, 2H); ^{13}C NMR (100 MHz, CD_3SOCD_3) δ = 179.53, 173.64, 148.21, 137.37, 135.17, 134.16, 132.96, 132.79, 129.11, 128.21, 128.12, 126.49, 126.23, 125.82, 48.45; HRMS (ESI-TOF): m/z calculated for $C_{17}H_{12}ClN_3O_3S$ $[M+Na]^+$, 396.0186; found 396.0177.

5-(4-Hydroxybenzylidene)-2-(benzylimino)thiazolidin-4-one (15f): Pale yellow solid; mp > 200 ºC; 192 mg, 31%, yield; IR (neat) ν_{max} = 3161, 2805, 1710, 1677, 1616, 1574, 1536 cm^{-1}; ^1H NMR (400 MHz, CD_3SOCD_3) δ 7.54 (s, 1H), 7.30-7.42 (m, 7H), 6.88 (d, 2H), 4.72 (s, 2H); ^{13}C NMR (100 MHz, CD_3SOCD_3) δ = 180.44, 176.16, 159.52, 137.75, 132.13, 131.99, 130.27, 129.07, 128.17, 128.01, 127.79, 126.27, 124.99, 116.62, 48.10; HRMS (ESI-TOF): m/z calculated for $C_{17}H_{14}N_2O_2S$ $[M+Na]^+$, 333.0674; found 333.0669.

5-(4-Methoxy-3-nitrobenzylidene)-2-(benzylimino)thiazolidin-4-one (15g): Yellow solid; mp > 200 ºC; 280 mg, 38% yield; IR (neat) ν_{max} = 3216, 3018, 1710, 1677, 1616, 1574, 1536 cm^{-1}; ^1H NMR (400 MHz, CD_3SOCD_3) δ 8.11 (s, 1H), 7.8803 (d, *J* = 8.86, 1H), 7.60 (s, 1H), 7.54 (d, *J* = 8.84, 1H), 7.30-7.37 (m, 5H), 4.73 (s, 2H), 3.97 (s, 3H); ^{13}C NMR (100 MHz, CD_3SOCD_3) δ = 179.87, 173.68, 153.00, 139.71, 137.61, 135.65, 129.48, 129.10, 128.19, 128.06, 127.85, 127.25, 127.09, 126.14, 115.72, 57.52, 48.42; HRMS (ESI-TOF): m/z calculated for $C_{18}H_{15}N_3O_4S$ $[M+Na]^+$, 392.0681; found 392.0673.

5-(4-Ethoxy-3-nitrobenzylidene)-2-(benzylimino)thiazolidin-4-one(15h): Pale yellow solid; mp > 200 ºC; 347 mg, 44% yield; IR (neat) ν_{max} = 3454, 2769, 1691, 1631, 1606, 1523 cm^{-1}; ^1H NMR (400 MHz, CD_3SOCD_3) δ 8.09 (s, 1H), 7.84 (d, *J* = 8.88, 1H), 7.63 (s, 1H), 7.52 (d, *J* = 8.88, 1H) 7.39-7.31 (m, 5H). 4.75 (s, 2H), 4.31 - 4.25 (m, 2H), 1.37 (t, *J* = 6.93, 3H); ^{13}C NMR (100 MHz, CD_3SOCD_3) δ 179.87, 173.79, 152.22, 140.00, 137.54, 135.49, 129.25, 129.10, 128.20, 128.08, 127.86, 127.43, 126.92, 126.11, 116.39, 66.01, 48.32, 14.74; HRMS (ESI-TOF): m/z calculated for $C_{19}H_{17}N_3O_4S$ $[M+Na]^+$, 406.0837; found 406.0832.

5-(3-Hydroxybenzylidene)-2-(benzylimino)thiazolidin-4-one (15i): Pale yellow solid; mp > 200 ºC; 186 mg, 31% yield; IR (neat) ν_{max} = 3278, 2813, 1715, 1686, 1624, 1609, 1590 cm^{-1}; ^1H NMR (400 MHz, CD_3SOCD_3) δ 7.50 (s, 1H), 7.38-7.27 (m, 6H), 6.99 (d, *J* = 7.32, 1H), 6.95 (s, 1H), 6.82 (d, *J* = 8.04, 1H); ^{13}C NMR (100 MHz, CD_3SOCD_3) δ = 180.09, 174.20, 158.30, 137.68, 135.70, 130.67, 129.87, 129.08, 128.97, 128.22, 128.04, 127.77, 121.21, 117.33, 116.00,115.90, 48.29; HRMS (ESI-TOF): m/z calculated for $C_{17}H_{14}N_2O_2S$ $[M+Na]^+$, 333.0674; found 333.0665.

5-(4-Fluorobenzylidene)-2-(benzylimino)thiazolidin-4-one (15j): Pale yellow solid; mp > 200 ºC; 232 mg, 37% yield; IR (neat) ν_{max} = 1710, 1686, 1627, 1610, 1597 cm^{-1}; ^1H NMR (400 MHz, CD_3SOCD_3) δ 7.64-7.60 (m, 3H), 7.40-7.30 (m, 7H), 4.74 (s, 2H); ^{13}C NMR (100 MHz, CD_3SOCD_3) δ = 180.03, 174.11, 164.08, 161.60, 137.55, 132.35, 132.21, 132.12, 131.12, 131.08, 129.10, 128.93, 128.90, 128.70, 128.22, 128.08, 127.80, 116.88, 116.67, 48.25; HRMS (ESI-TOF): m/z calculated for $C_{17}H_{13}FN_2OS$ $[M+Na]^+$, 335.0630; found 335.0623.

5-(3-ethoxy-4-hydroxybenzylidene)-2-(benzylimino)thiazolidin-4-one (15k): Pale yellow solid; mp 178-180 ºC; 294 mg, 41% yield; IR (neat) ν_{max} = 3524, 3354, 3061, 2976, 2931, 2753, 1681, 1633, 1610, 1587 cm^{-1}; ^1H NMR (400 MHz, $CDCl_3$) δ 7.47 (s, 1H), 7.11-7.23 (m, 5H), 6.89-6.91 (m, 2H), 6.76 (d, *J* = 8.12, 1H). 4.61 (s, 2H), 4.05-4.00 (m, 2H), 1.29 (m, 3H); ^{13}C NMR (100 MHz, CD_3SOCD_3) δ = 186.08, 179.20, 152.90, 151.08, 140.54, 135.93, 132.51, 132.40, 131.61, 131.54, 131.26, 129.75, 127.83, 127.78, 119.52, 117.91, 68.25, 17.61; HRMS (ESI-TOF): m/z calculated for $C_{19}H_{18}N_2O_3S$ $[M+Na]^+$, 377.0936; found 377.0928.

5-(3,4-Dimethoxybenzylidene)-2-(benzylimino)thiazolidin-4-one (15l): Pale yellow solid; mp > 200 ºC; 270 mg, 38% yield; IR (neat) ν_{max} = 3524, 2753, 1679, 1624, 1593 cm^{-1}; ^1H NMR (400 MHz, CD_3SOCD_3) δ 7.58 (s, 1H), 7.38-7.28 (m, 5H), 7.16-7.12 (m, 2H), 7.06 (d, *J* = 8.28, 1H), 4.72 (s, 2H), 3.42 (s, 6H); ^{13}C NMR (100 MHz, CD_3SOCD_3) δ = 180.31, 174.16, 150.71, 150.56, 149.35, 137.69, 137.55, 130.70, 130.20, 129.09, 129.06, 128.14, 128.07, 128.01, 127.93, 127.13, 126.92, 126.39, 123.26, 123.18, 113.55, 113.28, 112.50, 56.06, 56.00, 48.15; HRMS (ESI-TOF): m/z calculated for $C_{19}H_{18}N_2O_3S$ $[M+Na]^+$, 377.0936; found 377.0936.

5-(4-Methoxybenzylidene)-2-(benzylimino)thiazolidin-4-one (15m): Pale yellow solid; mp > 200 ºC; 177 mg, 27% yield; IR (neat) ν_{max} = 1710, 1667, 1637, 1598, 1571 cm^{-1}; ^1H NMR (400 MHz, CD_3SOCD_3) δ 7.54 (s, 1H), 7.39 (d, *J* = 8.68, 2H), 7.39-7.28 (m. 5H), 7.04 (d, *J* = 8.48, 2H), 4.75 (s, 2H), 3.75 (s, 3H); ^{13}C NMR (100 MHz, CD_3SOCD_3) δ = 180.40, 174.21, 160.80, 137.64, 131.75, 129.86, 129.08, 128.15, 128.05, 127.78, 126.80, 126.14, 115.24, 55.85, 48.14; HRMS (ESI-TOF): m/z calculated for $C_{18}H_{16}N_2O_2S$ $[M+Na]^+$, 347.0830; found 347.0864.

Acknowledgments

The authors thank Department of Science and Technology (DST), Govt. of India, New Delhi, India for financial support. The authors thank NIPER, S. A. S. Nagar for infrastructural Facilities and financial assistance. S.B thanks University Grant Commission (UGC), Govt. of India, New Delhi, India for financial assistance.

Supporting Information

Supporting information contains the docking pose of the hinge binding fragments, docking pose of the fragments binding to the polar region, binding pose of the compounds, quantum chemical information for tautomeric analysis, details of molecular dynamics, ^1H NMR and ^{13}C NMR spectra, experimental details of biochemical assay

References and notes

[1] A.K. Acharya, Y.A. Chang, G.O. Jones, J.E. Rice, J.L. Hedrick, H.W. Horn, R.M. Waymouth, Experimental and computational studies on the mechanism of zwitterionic ring-opening polymerization of delta-valerolactone with N-heterocyclic carbenes, J. Phys. Chem. B, 118 (2014) 6553-6560.

[2] a) A. Martinez, C. Gil, D.I. Perez, Glycogen synthase kinase 3 inhibitors in the next horizon for Alzheimer's disease treatment, Int. J. Alzheimers Dis., 2011 Article ID 280502, 280507 pages, 282011. doi:280510.284061/282011/280502; b) P. Cohen, M. Goedert, GSK-3 inhibitors: development and therapeutic potential, Nat. Rev. Drug. Discov., 3 (2004) 479-487; c) C.A. Grimes, R.S. Jope, The multifaceted roles of glycogen synthase kinase 3β in cellular signaling, Prog. Neurobiol., 65 (2001) 391-426; d) T. Kramer, B. Schmidt, F. Lo Monte, Small-Molecule Inhibitors of GSK-3: Structural Insights and Their Application to Alzheimer's Disease Models, International Journal of Alzheimer's Disease, 2012 (2012) 32.

[3] N. Embi, D.B. Rylatt, P. Cohen, Glycogen synthase kinase-3 from rabbit skeletal muscle. Separation from cyclic-AMP-dependent protein kinase and phosphorylase kinase, Eur. J. Biochem., 107 (1980) 519-527.
[4] J.R. Woodgett, P. Cohen, Multisite phosphorylation of glycogen synthase. Molecular basis for the substrate specificity of glycogen synthase kinase-3 and casein kinase-II (glycogen synthase kinase-5), Biochim. Biophys. Acta., 788 (1984) 339-347.
[5] a) E. Droucheau, A. Primot, V. Thomas, D. Mattei, M. Knockaert, C. Richardson, P. Sallicandro, P. Alano, A. Jafarshad, B. Baratte, C. Kunick, D. Parzy, L. Pearl, C. Doerig, L. Meijer, Plasmodium falciparum glycogen synthase kinase-3: molecular model, expression, intracellular localisation and selective inhibitors, Biochim. Biophys. Acta., 1697 (2004) 181-196; b) M. Mora-Santos, M.C. Limon-Mortes, S. Giraldez, J. Herrero-Ruiz, C. Saez, M.A. Japon, M. Tortolero, F. Romero, Glycogen synthase kinase-3beta (GSK3beta) negatively regulates PTTG1/human securin protein stability, and GSK3beta inactivation correlates with securin accumulation in breast tumors, J. Biol. Chem., 286 (2012) 30047-30056; c) I. Collins, Targeted small-molecule inhibitors of protein kinase B as anticancer agents, Anticancer Agents Med. Chem., 9 (2009) 32-50; d) J. Lee, M.S. Kim, The role of GSK-3 in glucose homeostasis and the development of insulin resistance, Diabetes Res. Clin. Pract., 77 Suppl 1 (2007) S49-57; e) T.D. Gould, Targeting glycogen synthase kinase-3 as an approach to develop novel mood-stabilising medications, Expert Opin. Ther. Targets, 10 (2006) 377-392; f) E.J. Henriksen, B.B. Dokken, Role of glycogen synthase kinase-3 in insulin resistance and type 2 diabetes, Curr. Drug. Targets, 7 (2006) 1435-1441; g) R. Boulahjar, A. Ouach, S. Bourg, P. Bonnet, O. Lozach, L. Meijer, C. Guguen-Guillouzo, R. Le Guevel, S. Lazar, M. Akssira, Y. Troin, G. Guillaumet, S. Routier, Advances in tetrahydropyrido[1,2-a]isoindolone (valmerins) series: Potent glycogen synthase kinase 3 and cyclin dependent kinase 5 inhibitors, Eur. J. Med. Chem., 101 (2015) 274-287.
[6] a) V. Palomo, D.I. Perez, C. Perez, J.A. Morales, I. Soteras, S. Alonso-Gil, A. Encinas, A. Castro, N.E. Campillo, A. Perez-Castillo, C. Gil, A. Martinez, 5-Imino-1,2,4-Thiadiazoles: First Small Molecules as Substrate Competitive Inhibitors of Glycogen Synthase Kinase 3, J. Med. Chem., 55 (2012) 1645-1661; b) A. Martinez, M. Alonso, A. Castro, C. Perez, F.J. Moreno, First non-ATP competitive glycogen synthase kinase 3β (GSK-3β) inhibitors: thiadiazolidinones (TDZD) as potential drugs for the treatment of Alzheimer's disease, J. Med. Chem., 45 (2002) 1292-1299; c) A. Martinez, M. Alonso, A. Castro, I. Dorronsoro, J.L. Gelpi, F.J. Luque, C. Perez, F.J. Moreno, SAR and 3D-QSAR Studies on Thiadiazolidinone Derivatives: Exploration of Structural Requirements for Glycogen Synthase Kinase 3 Inhibitors, J. Med. Chem., 48 (2005) 7103-7112.
[7] a) M.A. Khanfar, B.A. Asal, M. Mudit, A. Kaddoumi, K.A. El Sayed, The marine natural-derived inhibitors of glycogen synthase kinase-3β phenylmethylene hydantoins: In vitro and in vivo activities and pharmacophore modeling, Bioorg. Med. Chem., 17 (2009) 6032-6039; b) M.A. Khanfar, R.A. Hill, A. Kaddoumi, K.A. El Sayed, Discovery of novel GSK-3β inhibitors with potent *in vitro* and i*n vivo* activities and excellent brain permeability using combined ligand- and structure-based virtual screening, J. Med. Chem., 53 (2010) 8534-8545.
[8] a) M. Saitoh, J. Kunitomo, E. Kimura, Y. Hayase, H. Kobayashi, N. Uchiyama, T. Kawamoto, T. Tanaka, C.D. Mol, D.R. Dougan, G.S. Textor, G.P. Snell, F. Itoh, Design, synthesis and structure-activity relationships of 1,3,4-oxadiazole derivatives as novel inhibitors of glycogen synthase kinase-3β, Bioorg. Med. Chem. Lett., 17 (2009) 2017-2029; b) M. Saitoh, J. Kunitomo, E. Kimura, H. Iwashita, Y. Uno, T. Onishi, N. Uchiyama, T. Kawamoto, T. Tanaka, C.D. Mol, D.R. Dougan, G.P. Textor, G.P. Snell, M. Takizawa, F. Itoh, M. Kori, 2-{3-[4-(Alkylsulfinyl)phenyl]-1-benzofuran-5-yl}-5-methyl-1,3,4-oxadiazol e derivatives as novel inhibitors of glycogen synthase kinase-3β with good brain permeability, J. Med. Chem., 52 (2009) 6270-6286.
[9] a) S. Sestito, G. Nesi, S. Daniele, A. Martelli, M. Digiacomo, A. Borghini, D. Pietra, V. Calderone, A. Lapucci, M. Falasca, P. Parrella, A. Notarangelo, M.C. Breschi, M. Macchia, C. Martini, S. Rapposelli, Design and synthesis of 2-oxindole based multi-targeted inhibitors of PDK1/Akt signaling pathway for the treatment of glioblastoma multiforme, Eur. J Med. Chem., 105 (2015) 274-288; b) E. Moine, I. Dimier-Poisson, C. Enguehard-Gueiffier, C. Logé, M. Pénichon, N. Moiré, C. Delehouzé, B. Foll-Josselin, S. Ruchaud, S. Bach, A. Gueiffier, F. Debierre-Grockiego, C. Denevault-Sabourin, Development of new highly potent imidazo[1,2-b]pyridazines targeting Toxoplasma gondii calcium-dependent protein kinase 1, Eur. J. Med. Chem., 105 (2015) 80-105.
[10] F. Zuccotto, E. Ardini, E. Casale, M. Angiolini, Through the "gatekeeper door": exploiting the active kinase conformation, J. Med. Chem., 53 (2010) 2681-2694.
[11] A.P. Kozikowski, I.N. Gaisina, H. Yuan, P.A. Petukhov, S.Y. Blond, A. Fedolak, B. Caldarone, P. McGonigle, Structure-based design leads to the identification of lithium mimetics that block mania-like effects in rodents. possible new GSK-3β therapies for bipolar disorders, J. Am. Chem. Soc., 129 (2007) 8328-8332.
[12] a) P. Polychronopoulos, P. Magiatis, A.L. Skaltsounis, V. Myrianthopoulos, E. Mikros, A. Tarricone, A. Musacchio, S.M. Roe, L. Pearl, M. Leost, P. Greengard, L. Meijer, Structural Basis for the Synthesis of Indirubins as Potent and Selective Inhibitors of Glycogen Synthase Kinase-3 and Cyclin-Dependent Kinases, J. Med. Chem., 47 (2004) 935-946; b) A.P. Kozikowski, I.N. Gaisina, P.A. Petukhov, J. Sridhar, L.T. King, S.Y. Blond, T. Duka, M. Rusnak, A. Sidhu, Highly Potent and Specific GSK-3β inhibitors That Block tau Phosphorylation and Decrease alpha-Synuclein Protein Expression in a Cellular Model of Parkinson's disease, ChemMedChem, 1 (2006) 256-266.
[13] a) L. Meijer, A.L. Skaltsounis, P. Magiatis, P. Polychronopoulos, M. Knockaert, M. Leost, X.P. Ryan, C.A. Vonica, A. Brivanlou, R. Dajani, C. Crovace, C. Tarricone, A. Musacchio, S.M. Roe, L. Pearl, P. Greengard, GSK-3-Selective Inhibitors Derived from Tyrian Purple Indirubins, Chem. Biol., 10 (2003) 1255-1266; b) R. Bhat, Y. Xue, S. Berg, S. Hellberg, M. Ormo, Y. Nilsson, A.C. Radesater, E. Jerning, P.O. Markgren, T. Borgegard, M. Nylof, A. Gimenez-Cassina, F. Hernandez, J.J. Lucas, J. Diaz-Nido, J. Avila, Structural Insights and Biological Effects of Glycogen Synthase Kinase 3 Specific Inhibitor AR-A014418, J. Biol. Chem., 278 (2003) 45937-45945; c) P.M. Fischer, CDK versus GSK-3 inhibition: a purple haze no longer?, Chem. Biol., 10 (2003) 1144-1146.
[14] a) M. Arfeen, P.V. Bharatam, Design of glycogen synthase kinase-3 inhibitors: an overview on recent advancements, Curr. Pharm. Des., 19 (2013) 4755-4775; b) D.S. Patel, N. Dessalew, P. Iqbal, P.V. Bharatam, Structure-based approaches in the design of GSK-3 selective inhibitors, Curr. Protein Pept. Sci., 8 (2007) 352-364; c) M. Arfeen, R. Patel, T. Khan, P.V. Bharatam, Molecular dynamics simulation studies of GSK-3β ATP competitive inhibitors: understanding the factors contributing to selectivity, J. Biomol. Struct. Dyn., 33 (2015) 2578-2593.
[15] a) N. Singh, A. Tripathi, A. Tewari, R. Kumar, S. Saraf, Ulcerogenicity devoid novel non-steroidal anti-inflammatory agents (NSAIDS): syntheses, computational studies, and activity of 5-aryliden-2-imino-4-thiazolidinones, Med. Chem. Res., 24 (2015) 1927-1941; b) P. Eleftheriou, A. Geronikaki, D. Hadjipavlou-Litina, P. Vicini, O. Filz, D. Filimonov, V. Poroikov, S.S. Chaudhaery, K.K. Roy, A.K. Saxena, Fragment-based design, docking, synthesis, biological evaluation and structure-activity relationships of 2-benzo/benzisothiazolimino-5-aryliden-4-thiazolidinones as cycloxygenase-lipoxygenase inhibitors, Eur. J. Med. Chem., 47 (2012) 111-124.
[16] a) P. Vicini, A. Geronikaki, M. Incerti, F. Zani, J. Dearden, M. Hewitt, 2-Heteroarylimino-5-benzylidene-4-thiazolidinones analogues of 2-thiazolylimino-5-benzylidene-4-thiazolidinones with antimicrobial activity: Synthesis and structure–activity relationship, Bioorg. Med. Chem., 16 (2008) 3714-3724; b) I. Kucukguzel, G. Satilmis, K.R. Gurukumar, A. Basu, E. Tatar, D.B. Nichols, T.T. Talele, N. Kaushik-Basu, 2-Heteroarylimino-5-arylidene-4-thiazolidinones as a new class of non-nucleoside inhibitors of HCV NS5B polymerase, Eur. J. Med. Chem., 69 (2013) 931-941.
[17] A. Geronikaki, P. Eleftheriou, P. Vicini, I. Alam, A. Dixit, A.K. Saxena, 2-Thiazolylimino/Heteroarylimino-5-arylidene-4-thiazolidinones as New Agents with SHP-2 Inhibitory Action, J. Med. Chem., 51 (2008) 5221-5228.
[18] a) W.K. Coulibaly, L. Paquin, A. Benie, Y.A. Bekro, E. Durieux, L. Meijer, R.L. Guevel, A. Corlu, J.P. Bazureau, Synthesis of New N,N'-Bis(5-arylidene-4-oxo-4,5-dihydrothiazolidin-2-yl)piperazine Derivatives Under Microwave Irradiation and Preliminary Biological Evaluation, Sci. Pharm., 80 (2012) 825-836; b) M. Sarkis, D.N. Tran, S. Kolb, M.A. Miteva, B.O. Villoutreix, C. Garbay, E. Braud, Design and synthesis of novel bis-thiazolone derivatives as micromolar CDC25 phosphatase inhibitors: Effect of dimerisation on phosphatase inhibition, Bioorg. Med. Chem. Lett., 22 (2012) 7345-7350; c) A.A. Geronikaki, A.A. Lagunin, D.I. Hadjipavlou-Litina, P.T. Eleftheriou, D.A. Filimonov, V.V. Poroikov, I. Alam, A.K. Saxena, Computer-Aided Discovery of Anti-Inflammatory Thiazolidinones with Dual Cyclooxygenase/Lipoxygenase Inhibition, J. Med. Chem., 51 (2008) 1601-1609.
[19] J.A. Bertrand, S. Thieffine, A. Vulpetti, C. Cristiani, B. Valsasina, S. Knapp, H.M. Kalisz, M. Flocco, Structural characterization of the GSK-3β active site using selective and non-selective ATP-mimetic inhibitors, J. Mol. Biol., 333 (2003) 393-407.
[20] S. Berg, M. Bergh, S. Hellberg, K. Hogdin, Y. Lo-Alfredsson, P. Soderman, S. von Berg, T. Weigelt, M. Ormo, Y. Xue, J. Tucker, J. Neelissen, E. Jerning, Y. Nilsson, R. Bhat, Discovery of novel potent and highly selective glycogen synthase kinase-3beta (GSK3beta) inhibitors for Alzheimer's disease: design, synthesis, and characterization of pyrazines, J. Med. Chem., 55 (2012) 9107-9119.
[21] a) M.H. Bolli, S. Abele, C. Binkert, R. Bravo, S. Buchmann, D. Bur, J. Gatfield, P. Hess, C. Kohl, C. Mangold, B. Mathys, K. Menyhart, C. Müller, O. Nayler, M. Scherz, G. Schmidt, V. Sippel, B. Steiner, D. Strasser, A. Treiber, T. Weller, 2-Imino-thiazolidin-4-one Derivatives as Potent, Orally Active S1P1 Receptor Agonists, J. Med. Chem., 53 (2010) 4198-4211; b) G.H. Al-Ansary, M.A.H. Ismail, D.A. Abou El Ella, S. Eid, K.A.M. Abouzid,

Molecular design and synthesis of HCV inhibitors based on thiazolone scaffold, Eur. J Med. Chem., 68 (2013) 19-32.
[22] J.C. Thenmozhiyal, P.T.-H. Wong, W.-K. Chui, Anticonvulsant Activity of Phenylmethylenehydantoins: A Structure−Activity Relationship Study, J. Med. Chem, 47 (2004) 1527-1535.
[23] a) S.M. Rodems, B.D. Hamman, C. Lin, J. Zhao, S. Shah, D. Heidary, L. Makings, J.H. Stack, B.A. Pollok, A FRET-based assay platform for ultra-high density drug screening of protein kinases and phosphatases, Assay Drug Dev. Technol., 1 (2002) 9-19; b) C. Grutter, J.R. Simard, S.C. Mayer-Wrangowski, P.H. Schreier, J. Perez-Martin, A. Richters, M. Getlik, O. Gutbrod, C.A. Braun, M.E. Beck, D. Rauh, Targeting GSK3 from Ustilago maydis: type-II kinase inhibitors as potential antifungals, ACS Chem. Biol., 7 (2012) 1257-1267; c) F. Lo Monte, T. Kramer, J. Gu, U.R. Anumala, L. Marinelli, V. La Pietra, E. Novellino, B. Franco, D. Demedts, F. Van Leuven, A. Fuertes, J.M. Dominguez, B. Plotkin, H. Eldar-Finkelman, B. Schmidt, Identification of Glycogen Synthase Kinase-3 inhibitors with a selective sting for glycogen synthase kinase-3alpha, J. Med. Chem., 55 (2012) 4407-4424.
[24] C.M. Richardson, C.L. Nunns, D.S. Williamson, M.J. Parratt, P. Dokurno, R. Howes, J. Borgognoni, M.J. Drysdale, H. Finch, R.E. Hubbard, P.S. Jackson, P. Kierstan, G. Lentzen, J.D. Moore, J.B. Murray, H. Simmonite, A.E. Surgenor, C.J. Torrance, Discovery of a potent CDK2 inhibitor with a novel binding mode, using virtual screening and initial, structure-guided lead scoping, Bioor. Med. Chem. Lett., 17 (2007) 3880-3885.

List of Figures, Schemes and Table

Figure captions

Figure 1. Five membered rings reported as GSK-3β inhibitors (**1-13**).

Figure 2 Flow diagram representing the approach utilized for the design of 2-iminothiazolidin-4-one as GSK-3β ATP competitive inhibitors.

Figure 3. Different subpockets in the ATP binding region of GSK-3β along with AMP-PNP (Pdb code 1PYX).

Figure 4. Fragments considered for the binding to hinge region. Fragments were screened on the basis of interaction with Asp133 and Val135.

Figure 5. Fragments considered for the docking study into the polar binding region of ATP competitive inhibitors.

Figure 6. Structures of the designed first and second series of compounds.

Figure 7. Docked pose of **15g** and bar diagram represents the per residue wise decomposition analysis, residues on the X-axis, whereas Energy (kcal/mol) is on Y-axis.

Scheme captions

Scheme 1. Reagents, conditions and yields (i) CH_3COOH, CH_3COONa, reflux, 72 h, Yield 40-75%.

Scheme 2. Reagents, conditions and yields (i) DCM, NH_4OH, rt, 2 h, 81% and 83% (ii) EtOH, CH_3COONa, reflux, 6 h, 73% and 77% (iii) CH_3COOH, CH_3COONa, reflux, 72 h, 30-40%.

Table caption

Table 1. IC_{50} values for GSK-3β and percentage residual activity of CDK-2 for seven compounds at 2 μM Inhibitor concentration. The activity of CDK-2 in the absence of inhibitor was assigned the value of 100%.

Figures

Figure 1.

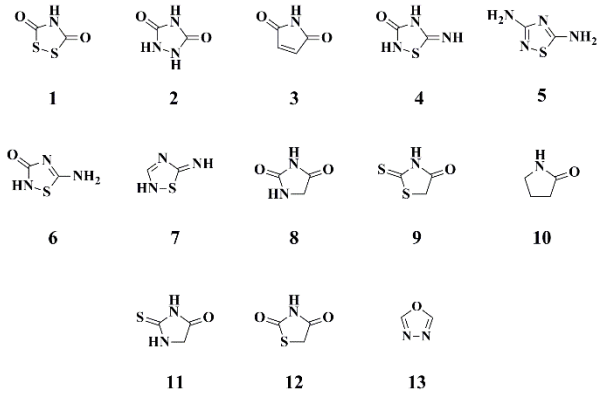

Figure 2.

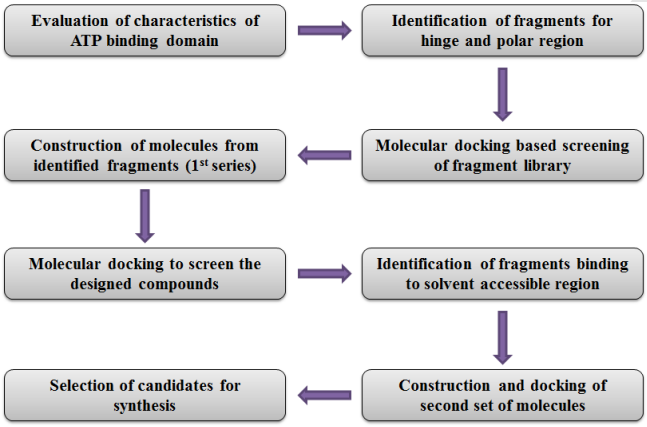

Figure 3.

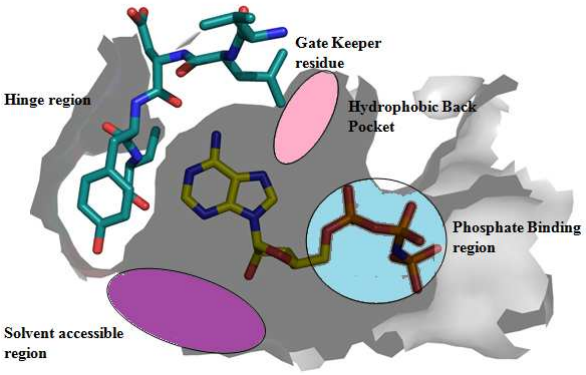

Figure 4.

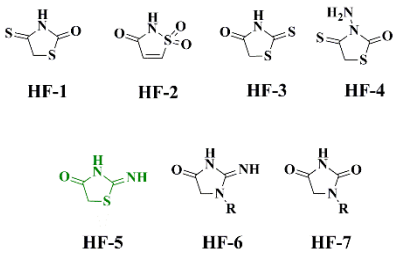

Figure 5.

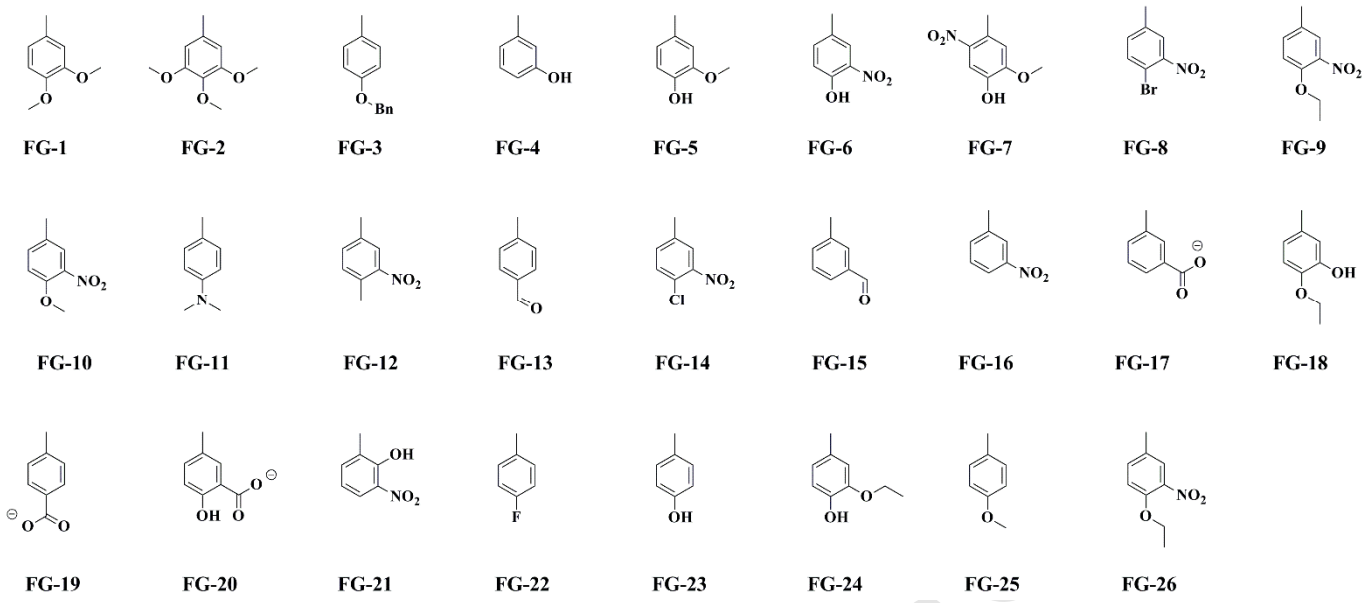

Figure 6.

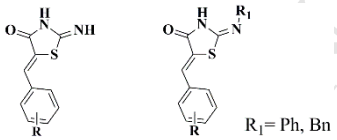

Figure 7.

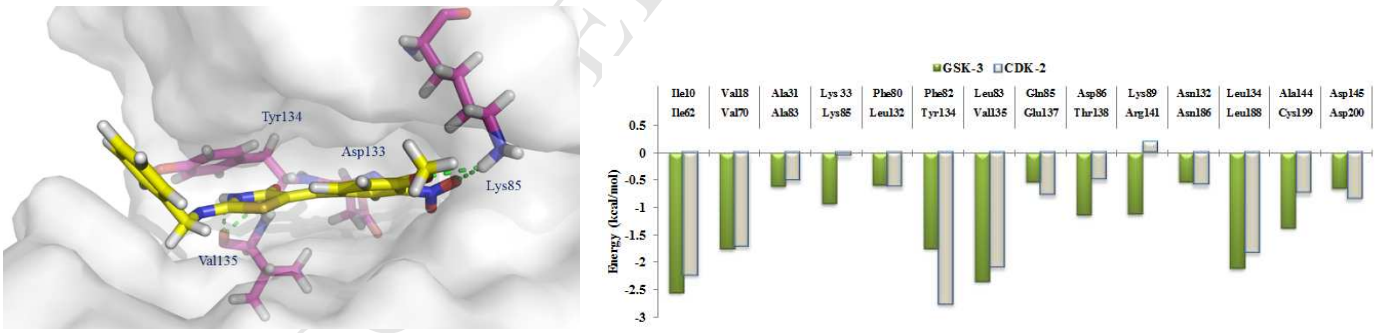

Schemes

Scheme 1.

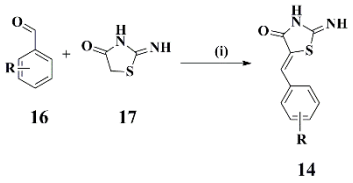

14a: R = 3,4-dimethoxy,
14b: R = 3,4,5-trimethoxy,
14c: R = 4-hydroxy-3-methoxy,
14d: R = 4-hydroxy-3-nitro,
14e: R = 4-bromo-3-nitro,
14f: R = 4-methoxy-3-nitro,
14g: R = 4-formyl,
14h: R = 4-chloro-3-nitro,
14i: R = 3-carboxylic acid,
14j: R = 3-ethoxy-4-hydroxy,
14k: R = 4-carboxylic acid,
14l: R = 4-hydroxy-3-carboxylic acid,

Scheme 2.

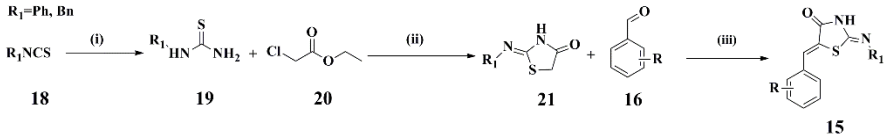

15a: R_1 = Ph, R = 4-hydroxy,
15b: R_1 = Ph, R = 4-fluoro,
15c: R_1 = Ph, R = 4-chloro,
15d: R_1 = Bn, R = 4-hydroxy-3-nitro,
15e R_1 = Bn, R = 4-chloro-3-nitro,
15f: R_1 = Bn, R = 4-hydroxy,
15g R_1 = Bn, R = 4-methoxy-3-nitro,
15h: R_1 = Bn, R = 4-ethoxy-3-nitro
15i: R_1 = Bn, R= 3-hydroxy
15j: R_1 = Bn, R = 4-fluoro
15k: R_1 = Bn, R = 3-ethoxy-4-hydroxy
15l: R_1 = Bn, R = 3,4-dimethoxy
15m: R_1 = Bn, R = 4-methoxy

Table

Table1.

Sr. No.	Compound	IC_{50} (nM)	% Res. Act.
1	**15a**	27.7	69.63
2	**15b**	40.0	68.93
3	**15e**	24.0	68.40
4	**15f**	27.1	63.23
5	**15g**	2.1	73.01
6	**15k**	51.7	39.10
7	**15l**	44.3	53.83

Highlights

1. A few selective GSK-3β Inhibitors were designed and synthesized: 5-benzylidene-2-iminothiazolidin-4-ones.
2. Structure Based Drug Design techniques were utilized employed to highlight the importance of 2-iminothialidin-4-one ring.
3. *In vitro* evaluation of 25 compounds resulted in the identification of nine compounds with activity in the lower nanomolar range (2.1-84.8 nM).
4. Six compounds showed selective GSK-3β inhibitory activity against CDK-2 at 2μM concentration.
5. MD simulation showed that residues like Lys85, Thr138, and Arg141 play crucial role in selective inhibition.